

# Influence of compositionally induced defects on the vibrational properties of device grade $\text{Cu}_2\text{ZnSnSe}_4$ absorbers for kesterite based solar cells

Mirjana Dimitrievska, Andrew Fairbrother, Edgardo Saucedo, Alejandro Pérez-Rodríguez, and Victor Izquierdo-Roca'

Citation: *Appl. Phys. Lett.* **106**, 073903 (2015); doi: 10.1063/1.4913262

View online: <http://dx.doi.org/10.1063/1.4913262>

View Table of Contents: <http://aip.scitation.org/toc/apl/106/7>

Published by the [American Institute of Physics](#)

---

## Articles you may be interested in

[Vibrational spectra and lattice thermal conductivity of kesterite-structured  \$\text{Cu}\_2\text{ZnSnS}\_4\$  and  \$\text{Cu}\_2\text{ZnSnSe}\_4\$](#)   
*Appl. Phys. Lett.* **3**, 041102041102 (2015); 10.1063/1.4917044

[Band tailing and efficiency limitation in kesterite solar cells](#)  
*Appl. Phys. Lett.* **103**, 103506103506 (2013); 10.1063/1.4820250

[A low-temperature order-disorder transition in  \$\text{Cu}\_2\text{ZnSnS}\_4\$  thin films](#)  
*Appl. Phys. Lett.* **104**, 041911041911 (2014); 10.1063/1.4863685

[Multiwavelength excitation Raman scattering study of polycrystalline kesterite  \$\text{Cu}\_2\text{ZnSnS}\_4\$  thin films](#)  
*Appl. Phys. Lett.* **104**, 021901021901 (2014); 10.1063/1.4861593

---



Small Conferences. BIG Ideas.

Applied Physics  
Reviews

SAVE THE DATE!  
**3D Bioprinting: Physical and Chemical Processes**  
May 2–3, 2017 • Winston Salem, NC, USA

## Influence of compositionally induced defects on the vibrational properties of device grade $\text{Cu}_2\text{ZnSnSe}_4$ absorbers for kesterite based solar cells

Mirjana Dimitrievska,<sup>1</sup> Andrew Fairbrother,<sup>1</sup> Edgardo Saucedo,<sup>1</sup> Alejandro Pérez-Rodríguez,<sup>1,2</sup> and Victor Izquierdo-Roca<sup>1,a)</sup>

<sup>1</sup>Catalonia Institute for Energy Research (IREC), Jardins de les Dones de Negre 1, 08930 Sant Adrià de Besòs, Spain

<sup>2</sup>IN2UB, Universitat de Barcelona, C. Martí Franquès 1, 08028 Barcelona, Spain

(Received 11 January 2015; accepted 9 February 2015; published online 17 February 2015)

This work presents a detailed analysis of the impact of compositionally induced defects on the vibrational properties of  $\text{Cu}_2\text{ZnSnSe}_4$  absorbers for kesterite based solar cells. Systematic changes in the intensity of the E and B modes located around the 170, 220, and 250  $\text{cm}^{-1}$  frequency regions, which involve mostly cation vibrations, were observed and analyzed in relation to the occurrence of different kinds of defect clusters involving  $\text{V}_{\text{Cu}}$ ,  $\text{Zn}_{\text{Cu}}$ ,  $\text{Zn}_{\text{Sn}}$ ,  $\text{Cu}_{\text{Zn}}$ , and  $\text{Sn}_{\text{Zn}}$  point defects. Additional changes are also interpreted in terms of the appearance of SnSe, ZnSe, and CuSe-like contributions at the 185 and 250  $\text{cm}^{-1}$  spectral regions, respectively. The sensitivity of the Raman measurements to the presence of these kinds of defects corroborates the potential of Raman scattering for point defect assessment in these systems. © 2015 AIP Publishing LLC. [<http://dx.doi.org/10.1063/1.4913262>]

Kesterite semiconductors such as  $\text{Cu}_2\text{ZnSnSe}_4$  (CZTSe) are drawing attention because of their ideal optical properties for photovoltaic applications, especially as light-absorbers constituted of earth-abundant elements for development of sustainable thin film photovoltaic technologies. Though relatively high energy conversion efficiencies have already been reached for these materials,<sup>1</sup> still little is known about the nature of defects in these compounds. Kesterites, as quaternary compounds, provide ample opportunities for material design; however, this also results in a higher probability for formation of intrinsic defects. Defect concentration is expected to influence the optoelectronic properties of these materials, therefore a better understanding is crucial for improvement of CZTSe-based solar cells. Because of the limited knowledge about defects, many experimental observations on behavior of these materials cannot be fully understood. For example, why the highest efficiency CZTSe solar cells are produced within a narrow interval of Cu-poor and Zn-rich compositions,<sup>2</sup> or why stoichiometric films have better p-type conductivity than non-stoichiometric ones.<sup>3</sup>

Theoretical simulations through first principle calculations<sup>3–5</sup> have given much needed insights on phase stability and defect formation in these materials, but experimental confirmation of these results and identification of different types of defects is still notably lacking. One possible technique that can help in resolving this issue is Raman spectroscopy, which is extremely sensitive to structural disorder, in this case defined as any kind of modification of the crystalline structure of the material. This includes point defects, such as vacancies, interstitials, and anti-sites, and other crystalline defects, like dislocations or grain boundaries. Presence of defects can lead to several types of changes in the Raman spectra, depending on their type and concentration.

Effects in the Raman spectra caused by presence of a high concentration of defects are usually related to changes in frequency, shape, and intensity of the main Raman active vibrational modes. For example, in kesterite  $\text{Cu}_2\text{ZnSnS}_4$ , asymmetry in the shape of the low frequency region of the main A modes has been observed, which is attributed to phonon confinement effects arising from loss of translational symmetry in the crystal caused by a high density of defects.<sup>6</sup> The extreme of this situation is an amorphous material, where lack of long-range order leads to a Raman spectrum that reflects the phonon density of states and wave vector selection rules no longer apply. In both cases, changes in the Raman spectra could be explained by activation of non-center phonons due to relaxation of the quasicrystalline momentum conservation law, which is caused when translational symmetry of the crystal lattice is broken.

In contrast, the presence of a small amount of defects usually does not induce big changes in the Raman spectra.<sup>7</sup> Since crystal symmetry is mostly preserved in this case, Raman selection rules are also preserved, meaning that no changes in the frequencies of Raman active modes are expected. For this kind of behavior, three possible changes can occur in Raman spectra due to defects:

- (1) Occurrence of defects in a crystalline material may cause local vibrational modes, which lead to the presence of additional, usually rather small features in the Raman spectra. Impurities could lead to these effects.<sup>8</sup>
- (2) Presence of defects leads to a reduction of phonon lifetime, leading to a symmetric broadening of the Raman peaks, as phonon lifetime is inversely proportional to the natural line-width of the Raman peaks.<sup>9,10</sup>
- (3) Changes in the intensity of the Raman peaks can occur because of changes in the chemical bonds among the atoms in the material. In some cases, defects could lead to breakage of certain bonds, while in others they can induce formation of new ones. This implies changes in

<sup>a)</sup>Email: vizquierdo@irec.cat

the values of elements of the polarizability tensors related to vibrational modes involving these bonds, which in turn leads to changes in intensity of the corresponding peaks.<sup>11</sup>

In this framework, this work presents a detailed analysis of the impact of different kinds of compositionally induced defects in the Raman spectra from device-grade CZTSe absorbers (maximum efficiency 6.9%). Presence of different defect types is induced by changes in the processing composition of the CZTSe film in a sample with about 200 solar cells, each cell with an incremental change in the absorber composition. Analysis of the optoelectronic properties of the solar cells corroborates the strong impact of these defects on the device performance. The evaluation of vibrational properties of the absorbers in the cells has led to the observation of a correlation among the intensity ratio of different Raman bands and different types of defects. This analysis achieves a deeper understanding of the nature of the vibrations involved in the different peaks from CZTSe Raman spectra and provides experimental procedures for Raman scattering assessment of the presence of different kinds of defects with strong impact on the optoelectronic properties of these solar cell absorbers.

For the present study, a CZTSe thin film with a lateral composition gradient ( $\text{Cu}/(\text{Zn} + \text{Sn})$  from 0.55 to 1.20 and  $\text{Zn}/\text{Sn}$  from 0.70 to 1.90) was prepared by selenization of a Cu-Zn-Sn precursor film deposited by DC-magnetron sputtering.<sup>12</sup> The film was made into solar cell devices with a CdS/ZnO/ZnO:Al window layer and then mechanically scribed to form  $\sim 200$  cells  $3 \times 3 \text{ mm}^2$  in size, isolating each solar cell and dividing the graded film into small regions of relatively constant composition with which to correlate material and device properties. J-V characterization was made with an AAA Abet 3000 Solar Simulator, while compositional characterization of film was done by X-ray fluorescence spectroscopy (Fischerscope XVD). Raman scattering measurements were performed with 532.0 nm excitation using a LabRam HR800-UV and 457.9 nm excitation with T64000 Horiba-Jobin Yvon spectrometers.<sup>13</sup> All Raman spectra were acquired after the fabrication of the solar cell devices from which the CdS/ZnO/ZnO:Al window layer was removed using a dilute HCl solution.

Figure 1 shows a pseudo-ternary phase diagram of  $\text{Cu}_2\text{Se-ZnSe-SnSe}_2$  showing device efficiency with dependence on composition. Solid lines indicate the most expected secondary phases ( $\text{Cu}_2\text{Se}$ ,  $\text{ZnSe}$ , and  $\text{SnSe}_2$ ) and charge compensated point defect clusters: the A-type line corresponds to  $[\text{Zn}_{\text{Cu}} + \text{V}_{\text{Cu}}]$  defect complexes, the B-type line to  $[2\text{Zn}_{\text{Cu}} + \text{Zn}_{\text{Sn}}]$ , the C-type line to  $[2\text{Cu}_{\text{Zn}} + \text{Sn}_{\text{Zn}}]$ , and the D-type line to  $[\text{Cu}_{\text{Zn}} + \text{Cu}_i]$ .<sup>14</sup> The stoichiometric point is given by the intersection of these lines. For a composition between two secondary phase lines, a mixture of CZTSe and these two secondary phases would be expected, as well as different point defects and defect clusters. Note that D-type defect clusters were not investigated in this work due to lack of cells corresponding to that composition.

A maximum device efficiency of 6.9% is obtained, together with one of the highest reported open circuit voltage values (411 mV) for this compound.<sup>15,16</sup> The maximum values

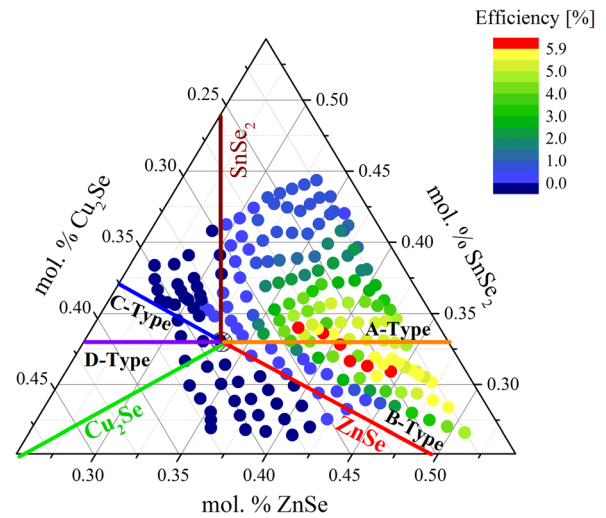


FIG. 1. Compositional dependence of device efficiency shown in a pseudo-ternary  $\text{Cu}_2\text{Se-ZnSe-SnSe}_2$  phase diagram for CZTSe solar cells; colored lines indicate expected secondary phases or defect clusters for a given region.

of the optoelectronic properties are achieved for a very narrow interval of compositions around  $\text{Cu}/(\text{Zn} + \text{Sn}) \approx 0.74$  and  $\text{Zn}/\text{Sn} \approx 1.23$ , which agree with previously reported results.<sup>2</sup> More detailed investigation of the optoelectronic properties with composition is presented elsewhere.<sup>12</sup>

In order to compare the influence of different defect clusters on the Raman modes, identification of peak positions and their symmetry assignment are necessary. Identification of peak positions of the stoichiometric CZTSe cell ( $\text{Cu}/(\text{Zn} + \text{Sn}) = 1.01$  and  $\text{Zn}/\text{Sn} = 1.00$ ) was done by simultaneous fitting of the Raman spectra with Lorentzian curves. The position of each Raman peak with the symmetry assignment is presented in Table I, which also contains theoretical calculations<sup>17</sup> and previously reported experimental data.<sup>18</sup> The symmetry assignment of Raman modes was done by

TABLE I. Frequency (in  $\text{cm}^{-1}$ ) of peaks from simultaneous fitting of Raman spectra of the stoichiometric CZTSe thin film and proposed mode symmetry assignment. These are compared with theoretical predictions<sup>17</sup> and reported experimental data.<sup>18</sup>

This work		Theoretical predictions	Experimentally reported
RS <sup>a</sup> ( $\text{cm}^{-1}$ )	Sym <sup>b</sup>	RS <sup>c</sup> ( $\text{cm}^{-1}$ )	RS <sup>d</sup> ( $\text{cm}^{-1}$ )
156.9	B	156.7 B(TO)/157.3 B(LO)	157 B(TO/LO)
171.9	A	162.8 A	170 A
174.5	A	166.5 A	174 A
177.4	B	175.3 B(TO)/178.7 B(LO)	178 B(TO/LO)
192.0	E	179.0 E(TO)/180.5 E(LO)	189 E(TO/LO)
196.8	A	186.3 A	196 A
220.6	E	199.8 E(TO)	224 E(TO)
231.9	E	202.8 E(LO)	231E(LO)
234.2	B	204.2 B(TO)	235 B(TO)
239.7	B	205.4 B(LO)	239B(LO)
248.3	B	227.1 B(TO)	245B(TO)
250.8	B	228.8 B(LO)	250 B(LO)

<sup>a</sup>RS is the Raman shift from this work.

<sup>b</sup>Sym is the symmetry proposed in this work.

<sup>c</sup>RS is the Raman shift reported in Ref. 17.

<sup>d</sup>RS is the Raman shift reported in Ref. 18.

comparing the experimentally obtained frequencies with the reported references as well as applying the rules<sup>13</sup> for the mode behavior to polarization measurements performed on this sample. It can be concluded that peak positions in Table I are in good agreement with the previous work.

Figures 2(a)–2(c) show the Raman spectra measured on samples that were selected with compositions following the lines corresponding to the A-, B-, and C-type of defect clusters. All Raman peaks observed in the spectra shown in these figures are attributed to the kesterite CZTSe phase, with peak positions in agreement with Table I. Raman characterization of these samples shows that formation of surface Sn-Se secondary phases takes place only in the region corresponding to  $\text{Cu}/(\text{Zn} + \text{Sn}) < 0.80$  and  $\text{Zn}/\text{Sn} < 0.95$  and has not been observed on the surface of any of the samples presented in Figure 2. In addition, Cu-Se binary phases have not been observed on the surface of any of the cells in this work. On the other hand, formation of ZnSe surface secondary phases has been observed, mainly in Zn-rich cells, detected with measurements with 457.9 nm excitation, which correspond to resonant excitation conditions for this compound.<sup>19</sup> Nevertheless, comparison of Raman spectra measured with 532 nm excitation from cells with and without ZnSe secondary phases indicates the absence of its Raman contribution in the  $250 \text{ cm}^{-1}$  spectral region. The low sensitivity of the Raman scattering measurements performed with 532 nm excitation to the presence of ZnSe secondary phases is related to low optical absorption of green photons in this compound, in contrast with very high optical absorption of CZTSe. This is also an indication of the low overall amount of ZnSe formed on the surface of the samples investigated. Accordingly, changes in this spectral region of the Raman spectra measured with 532 nm excitation from samples with different compositions cannot be attributed to the presence of ZnSe, in agreement with the previous work showing Raman analysis before and after ZnSe etching.<sup>20</sup>

Figure 2(a) presents a comparison of Raman spectra for samples corresponding to different compositions when moving along the A-type defect line ( $[\text{Zn}_{\text{Cu}} + \text{V}_{\text{Cu}}]$ ) in the direction away from the stoichiometric point. Frequencies of the modes are not affected with this kind of compositional change, which implies that the concentration of defects in this region is not so high as to cause a notable overall distortion of the crystalline lattice. Additionally, no significant changes in the main A mode centered at  $196 \text{ cm}^{-1}$  are observed. Since this mode is attributed to only anion vibrations,<sup>21</sup> changes in its frequency and peak shape are usually correlated to the crystal quality of the absorber,<sup>6</sup> again confirming that no significant degradation of overall crystal quality of CZTSe is expected for this compositional interval. However, a systematic decrease in relative intensity of peaks around the  $170 \text{ cm}^{-1}$  spectral region is observed. This region corresponds to two A symmetry modes and two B symmetry modes. Since the A modes correspond to only Se vibrations, no changes in their intensity are expected with changes in cation composition. On the other side, theoretical simulations<sup>21</sup> indicate that B modes in this region correspond mostly to cation vibrations, in particular, to vibrations of Cu/Zn and Cu/Sn atomic planes. Considering that along the A-type defect compositional line, formation of  $[\text{Zn}_{\text{Cu}} + \text{V}_{\text{Cu}}]$  defect clusters is promoted, it can be concluded that Cu/Zn and Cu/Sn atomic planes are going to be affected: with an increase in concentration of  $[\text{Zn}_{\text{Cu}} + \text{V}_{\text{Cu}}]$  defects clusters, there will be a decrease in the number of Cu/Zn and Cu/Sn vibration units. This is consistent with a decrease in overall relative intensity of the B modes, in agreement with the experimental observations. This is also consistent with the fitting of the spectra that can be done keeping a constant Lorentzian contribution for the A modes in this spectral region.

Figure 2(b) shows a comparison of Raman spectra measured for samples along the B-type defect line ( $[\text{Zn}_{\text{Cu}} +$

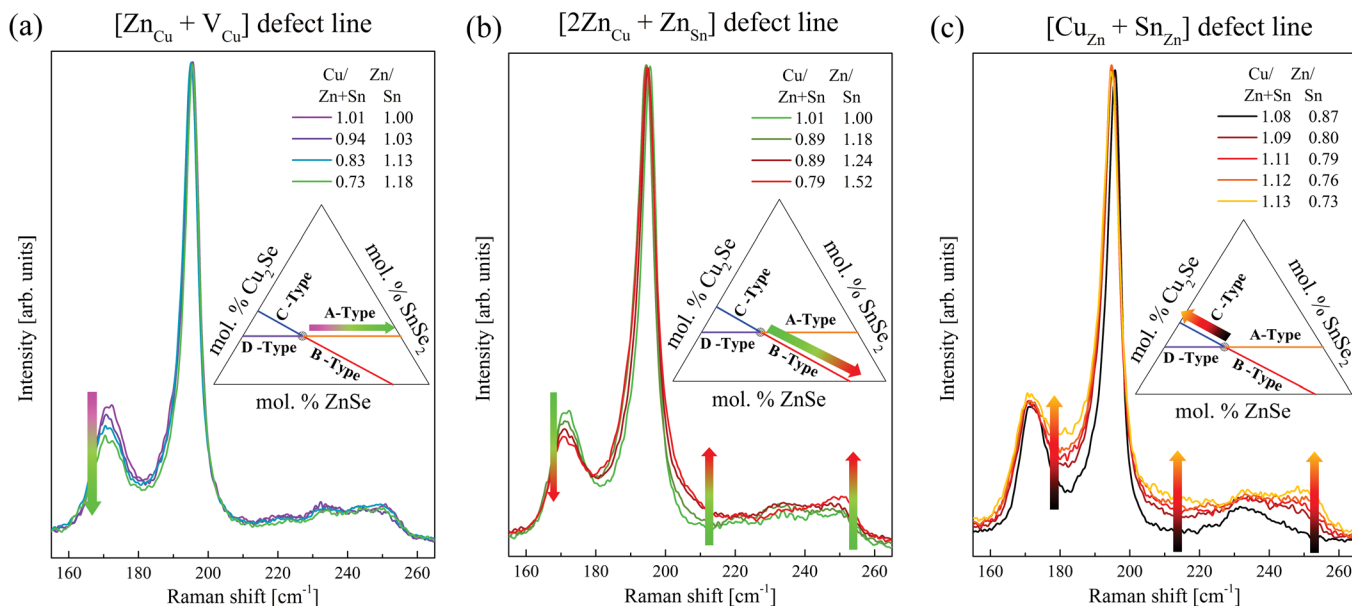


FIG. 2. Comparison of Raman spectra measured from samples with compositions corresponding to different defect lines: (a) A-type, (b) B-type, and (c) C-type. All Raman spectra are measured with 532 nm excitation wavelength. The arrows indicate changes in the intensity of the modes with the change in the composition in the directions shown on the ternary diagram.

$Zn_{Sn}$ ), again moving away from the stoichiometric point. As in the previous case, the frequency of the main A modes is not affected by this kind of compositional change. There are, however, strong changes in the relative intensity of the peaks around the 170, 215, and  $250\text{ cm}^{-1}$  frequency regions. Two defect types,  $Zn_{Cu}$  and  $Zn_{Sn}$ , are expected in this compositional range. A decrease in Cu content and increase in Zn content, which promotes  $Zn_{Cu}$  defect formation, are likely responsible for the decrease in relative intensity of the B symmetry modes around  $170\text{ cm}^{-1}$ , as explained in the previous case of A-type defects clusters. Additionally, increase in Zn content is also accompanied by an increase in the relative intensity of the spectral contribution at the  $250\text{ cm}^{-1}$  frequency region. This can be explained by taking into account the increase in density of  $Zn_{Cu}$  anti-sites, which leads to an increase in the number of Zn-Se bonds and, consequently, to an enrichment in the amount of Zn atoms surrounding Se anions in the lattice. This likely leads to the appearance of a ZnSe-like contribution that is expected at  $250\text{ cm}^{-1}$ .<sup>22</sup> An additional contribution to the intensity increase of this region can also be related to the increase in density of  $Zn_{Sn}$  anti-sites, which leads to transformation of the -Sn-Se-Cu-Se-Sn-vibrational chains into  $-Zn_{Sn}\text{-Se-Cu-Se-Zn}_{Sn}\text{-}$ , for which vibrations are also expected in the  $250\text{ cm}^{-1}$  region,<sup>21</sup> experimentally identified as a B mode. According to the theoretical analysis,<sup>21</sup> -Sn-Se-Cu-Se-Sn- vibrations are expected at a frequency of  $211\text{ cm}^{-1}$ . The proximity of this value with that of the E symmetry CZTSe mode experimentally observed at  $220\text{ cm}^{-1}$  leads to the identification of this mode with the vibrations of the -Sn-Se-Cu-Se-Sn- chains. The expected decrease in the relative intensity of this peak with the increase of  $Zn_{Sn}$  anti-sites is likely compensated by symmetric broadening of the main A mode at  $196\text{ cm}^{-1}$ , due to reduction in the phonon lifetime occurring at higher defect densities. This would lead to an overall increase in the relative intensity of this spectral contribution, in agreement with experimental observations shown in Figure 2(b).

Figure 2(c) presents the comparison of the Raman spectra measured from samples with compositions corresponding to the C-type defect line ( $[2Cu_{Zn} + Sn_{Zn}]$ ) when moving away from the stoichiometric point. As in the other cases, the frequency of the main A modes is unaffected by this compositional change. The most pronounced changes in the relative intensity of modes are observed in the frequency regions around 185, 220, and  $250\text{ cm}^{-1}$ . As this is a compositional region with a high probability of formation of  $[2Cu_{Zn} + Sn_{Zn}]$  defect clusters, increase in the relative intensity of the spectral contributions around the 185 and  $220\text{ cm}^{-1}$  regions could be related to the increase in density of  $Sn_{Zn}$  anti-sites. Increase in the density of  $Sn_{Zn}$  anti-sites would lead to an exchange of Zn by Sn in the -Cu-Se-Zn-Se-Cu-vibrational chains, equivalent to the -Zn-Se-Cu-Se-Zn-chains with vibrations identified as B symmetry mode at  $250\text{ cm}^{-1}$ , thus becoming  $-Cu\text{-Se-Sn}_{Zn}\text{-Se-Cu-}$ , that are equivalent to the -Sn-Se-Cu-Se-Sn- chains with vibrations identified as E mode at the  $220\text{ cm}^{-1}$  frequency region. This would explain the increase in the contribution at  $220\text{ cm}^{-1}$ . In addition, the changes of the spectra around the  $185\text{ cm}^{-1}$  frequency region can also be explained by taking into account the expected increase in the number of Sn-Se bonds, which would lead to

the appearance of a SnSe-like peak reported to be in this region.<sup>23</sup> On the other hand, the decrease expected in the  $250\text{ cm}^{-1}$  region because of the conversion of the B symmetry mode vibrations to the E symmetry one at  $220\text{ cm}^{-1}$  is likely compensated by the increase in density of  $Cu_{Zn}$  anti-sites. This would lead to a corresponding increase of Cu-Se bonds, with a subsequent enrichment of the amount of Cu atoms surrounding the Se anions in the lattice. This likely leads to the appearance of a CuSe-like contribution, as CuSe has a main vibrational peak at  $260\text{ cm}^{-1}$ .<sup>24</sup> However, differences in the local masses around the Se atoms likely lead to a red shift in the observed frequency of this contribution to the  $250\text{ cm}^{-1}$  spectral region. Finally, it is interesting to remark that the absence of changes in the spectral region around  $170\text{ cm}^{-1}$  in Figure 2(c) agrees with the assignment of the changes observed in this spectral region in Figures 2(a) and 2(b) to the occurrence of  $Zn_{Cu}$  and  $V_{Cu}$  defects, because the formation of these defects is inhibited for C-type absorbers.

In conclusion, changes observed in Raman spectra from samples grown with varied compositions which favor the formation of different kinds of defects can be explained by the following impact of  $V_{Cu}$ ,  $Zn_{Cu}$ ,  $Zn_{Sn}$ ,  $Cu_{Zn}$ , and  $Sn_{Zn}$  point defects:

- (1) Presence of  $V_{Cu}$  and  $Zn_{Cu}$  point defects induces a decrease in intensity of the B symmetry modes around  $170\text{ cm}^{-1}$  related to the vibrations in Cu/Zn and Cu/Sn planes (i.e., a decrease of Cu/Zn and Cu/Sn vibrational units).
- (2) Presence of  $Zn_{Sn}$  point defects lead to appearance of an additional ZnSe-like contribution at  $250\text{ cm}^{-1}$  and conversion from E symmetry modes at the  $220\text{ cm}^{-1}$  spectral region to B symmetry modes at the  $250\text{ cm}^{-1}$  spectral region.
- (3) Presence of  $Cu_{Zn}$  point defects lead to appearance of an additional CuSe-like contribution at the  $250\text{ cm}^{-1}$  frequency region.
- (4) Presence of  $Sn_{Zn}$  point defects lead to appearance of an additional SnSe-like contribution around the  $185\text{ cm}^{-1}$  frequency region and to conversion of B symmetry vibrational modes at the  $250\text{ cm}^{-1}$  spectral region into E symmetry vibrational modes at the  $220\text{ cm}^{-1}$  frequency region.

These results confirm the potential of Raman scattering for advanced characterization of absorbers in kesterite-based solar cells and corroborate the sensitivity of the Raman spectra from CZTSe device grade layers to the different kinds of point defects that are relevant for performance of solar cells. Systematic analysis of different spectral regions related to vibration of the different cations in the crystal gives a way for analysis of the processes in terms of point defect formation, which is especially relevant for further optimization of these technologies.

The research leading to these results has received funding from the People Program (Marie Curie Actions) of the European Union's Seventh Framework Program FP7/2007-2013/under REA Grant Agreement No. 316488 (KESTCELLS). Authors from IREC and IN<sup>2</sup>UB belong to

the M-2E (Electronic Materials for Energy) Consolidated Research Group and the XaRMAE Network of Excellence on Materials for Energy of the “Generalitat de Catalunya.” E.S. thanks the Government of Spain for the “Ramon y Cajal” fellowship (RYC-2011-09212) and V.I.-R. for the “Juan de la Cierva” fellowship (JCI-2011-10782) and A.F. thanks the Spanish Government for the FPU Fellowship (FPU12/05508).

- <sup>1</sup>W. Wang, M. T. Winkler, O. Gunawan, T. Gokmen, T. K. Todorov, Y. Zhu, and D. B. Mitzi, *Adv. Energy Mater.* **4**, 1301465 (2014).  
<sup>2</sup>H. Katagiri, *Thin Solid Films* **480–481**, 426 (2005).  
<sup>3</sup>S. Chen, A. Walsh, X.-G. Gong, and S.-H. Wei, *Adv. Mater.* **25**, 1522 (2013).  
<sup>4</sup>S. Chen, X. G. Gong, A. Walsh, and S.-H. Wei, *Appl. Phys. Lett.* **96**, 021902 (2010).  
<sup>5</sup>S. Chen, J.-H. Yang, X. G. Gong, A. Walsh, and S.-H. Wei, *Phys. Rev. B* **81**, 245204 (2010).  
<sup>6</sup>M. Dimitrievska, A. Fairbrother, A. Pérez-Rodríguez, E. Saucedo, and V. Izquierdo-Roca, *Acta Mater.* **70**, 272 (2014).  
<sup>7</sup>U. Rau, D. Abou-Ras, and T. Kirchartz, *Advanced Characterization Techniques for Thin Film Solar Cells* (John Wiley & Sons, 2011).  
<sup>8</sup>P. Panpech, S. Vijarnwannaluk, S. Sanorpim, W. Ono, F. Nakajima, R. Katayama, and K. Onabe, *J. Cryst. Growth* **298**, 107 (2007).  
<sup>9</sup>N. Kazemi-Zanjani, E. Kergrene, L. Liu, T.-K. Sham, and F. Lagugné-Labarthe, *Sensors* **13**, 12744 (2013).  
<sup>10</sup>T. B. Ivetić, M. R. Dimitrievska, N. L. Finčur, L. R. Đačanin, I. O. Gúth, B. F. Abramović, and S. R. Lukić-Petrović, *Ceram. Int.* **40**, 1545 (2014).  
<sup>11</sup>L. G. Cancado, A. Jorio, E. H. M. Ferreira, F. Stavale, C. A. Achete, R. B. Capaz, M. V. O. Moutinho, A. Lombardo, T. S. Kulmala, and A. C. Ferrari, *Nano Lett.* **11**, 3190 (2011).

- <sup>12</sup>M. Dimitrievska, A. Fairbrother, V. Izquierdo-Roca, A. Perez-Rodríguez, and E. Saucedo, in *40th IEEE Photovoltaic Specialist Conference (PVSC)* (2014), pp. 2307–2309.  
<sup>13</sup>M. Dimitrievska, A. Fairbrother, X. Fontané, T. Jawhari, V. Izquierdo-Roca, E. Saucedo, and A. Pérez-Rodríguez, *Appl. Phys. Lett.* **104**, 021901 (2014).  
<sup>14</sup>A. Lafond, L. Choubrac, C. Guillot-Deudon, P. Deniard, and S. Jobic, *Z. Anorg. Allg. Chem.* **638**, 2571 (2012).  
<sup>15</sup>Y. Sanchez, M. Neuschitzer, M. Dimitrievska, M. Espindola-Rodríguez, J. Lopez-Garcia, V. Izquierdo-Roca, O. Vigil-Galan, and E. Saucedo, in *40th IEEE Photovoltaic Specialist Conference (PVSC)* (2014), pp. 0417–0420.  
<sup>16</sup>Y. S. Lee, T. Gershon, O. Gunawan, T. K. Todorov, T. Gokmen, Y. Virgus, and S. Guha, “Cu<sub>2</sub>ZnSnSe<sub>4</sub> thin-film solar cells by thermal co-evaporation with 11.6% efficiency and improved minority carrier diffusion length,” *Adv. Energy Mater.* (published online, 2014).  
<sup>17</sup>A. Khare, B. Himmetoglu, M. Cococcioni, and E. S. Aydil, *J. Appl. Phys.* **111**, 123704 (2012).  
<sup>18</sup>M. Guc, S. Levchenko, V. Izquierdo-Roca, X. Fontané, E. Arushanov, and A. Pérez-Rodríguez, *J. Appl. Phys.* **114**, 193514 (2013).  
<sup>19</sup>A. Fairbrother, X. Fontané, V. Izquierdo-Roca, M. Placidi, D. Sylla, M. Espindola-Rodríguez, S. López-Mariño, F. A. Pulgarín, O. Vigil-Galán, A. Pérez-Rodríguez, and E. Saucedo, *Prog. Photovoltaics* **22**, 479 (2014).  
<sup>20</sup>S. López-Marino, Y. Sánchez, M. Placidi, A. Fairbrother, M. Espindola-Rodríguez, X. Fontané, V. Izquierdo-Roca, J. López-García, L. Calvo-Barrio, A. Pérez-Rodríguez, and E. Saucedo, *Chem. - Eur. J.* **19**, 14814 (2013).  
<sup>21</sup>N. B. Mortazavi Amiri and A. Postnikov, *Phys. Rev. B* **82**, 205204 (2010).  
<sup>22</sup>A. Redinger, K. Hônes, X. Fontané, V. Izquierdo-Roca, E. Saucedo, N. Valle, A. Pérez-Rodríguez, and S. Siebentritt, *Appl. Phys. Lett.* **98**, 101907 (2011).  
<sup>23</sup>T. Fukunaga, S. Sugai, T. Kinoshita, and K. Murase, *Solid State Commun.* **38**, 1049 (1981).  
<sup>24</sup>M. Ishii, K. Shibata, and H. Nozaki, *J. Solid State Chem.* **105**, 504 (1993).